JOURNAL OF GUIDANCE, CONTROL, AND DYNAMICS
Vol. 25, No. 4, July–August 2002

Control of Hovering Spacecraft Using Altimetry

S. Sawai,* D. J. Scheeres,† and S. B. Broschart‡
University of Michigan, Ann Arbor, Michigan 48109-2140

The control of a spacecraft hovering over a rotating small body, such as an asteroid or comet, is analyzed. The effect of closed-loop control strategies on the overall stability of hovering spacecraft trajectories is considered. We characterize the ability of one-dimensional altimetry measurements to stabilize a hovering spacecraft and find some ideal control methodologies that yield stable hovering trajectories. These ideas are developed for the ideal case of a uniformly rotating spherical small body and then are applied to a rotating ellipsoid and a rotating model of the asteroid Castalia. Application of this control approach to hovering over a nonuniformly rotating body is also analyzed. Finally, the stability of translational motions over an asteroid with active hovering control is studied and shown to be similar, in some cases, to hovering over a uniformly rotating body. The necessary modifications to the measurement and control laws for these more general cases are characterized as well.

Introduction

PERFORMING scientific explorations of small bodies, such as asteroids and comets, can be simplified, in many cases, by abandoning an orbital approach[1] in favor of a hovering approach.[2] In the hovering approach, the spacecraft thrusts continuously (or nearly continuously) to null out gravitational and rotational accelerations, fixing its position in the body-fixed frame. Such an approach to small-body exploration would make it possible to obtain high-resolution measurements, and even samples, from multiple sites over the body surface without having to make complicated transitions from orbital to body-fixed trajectories between each near-surface observation period. Some future missions, including MUSES-C, the Japanese asteroid sample return mission,[3] plan to hover over small bodies. The implementation of such hovering trajectories is not trivial, however, because they are fundamentally unstable[2] and may involve the complex interplay of several navigation sensors and control actuators to implement.

In this paper, we investigate the feasibility of simplifying the navigation of these trajectories by applying a simple control law to stabilize the hovering trajectory. If the hovering trajectory can be stabilized, the complexity of the entire navigation problem can be similarly reduced. Ideally, the stabilizing control loop can then run in the background while a more sophisticated control loop is used to drive the hovering spacecraft over the small-body surface. These higher-level control laws will be simpler to implement and characterize if the underlying stability of the hovering trajectory is ensured.

Our proposed approach to stabilizing the hovering trajectory uses a single altimeter and thrusting direction. By tightly controlling the spacecraft altitude along the gravitational direction, we show that it is possible to completely stabilize the hovering trajectory in most cases of interest. We define and analyze the stability and implementation of this control for a spacecraft hovering over a rotating sphere, ellipsoid, and a generalized shape based on the asteroid Castalia.[4] We treat hovering over uniformly rotating bodies, as well as nonuniformly rotating bodies. We note that our control law does not stabilize a hovering trajectory everywhere in space and, in general, only stabilizes motion for hovering less than a characteristic altitude related to resonant motion about the asteroid. Limited simulations of our approach are presented to verify its utility.

Following our discussion of stationary hovering, the implementation and stability of guidance laws for translational motion over the surface of a small body are investigated. For translational motion over large angular distances, we define a contour-line maneuver. In this case, the hovering spacecraft maintains altitude to keep its gravitational potential constant and is given an additional rotation rate relative to the central body, with the nominal closed-loop control being updated as a function of position. For the case of traveling over a point mass, this guidance law is equivalent to the hovering problem, although we see that there are preferential directions in which to implement these transfers. When a nonspherical body is modeled, the stability of these transfers must be modeled numerically, although results from translation over a spherical body can be used to guide the analysis.

Consideration of Controller Type

Previous work[2] assumed open-loop control to cancel the centrifugal force and gravitational attraction to maintain the hovering position of a spacecraft. Control thrust was added as a quasi-continuous constant acceleration to balance the residual acceleration of the spacecraft at its prescribed hovering point. However, these hovering equilibrium points are not stable for most positions and require some closed-loop control to maintain. If the spacecraft is equipped with a full dimensional controller, these hovering trajectories can always be stabilized. However, such a controller may require extensive spacecraft resources.

In this paper, we assume a very simple closed-loop control to stabilize the open-loop hovering trajectories. In particular, we assume tight controllers that keep the altimetry output constant. With such a simple control logic, hovering can be easily implemented with an altimeter directed in the proper direction. The sensing and control direction of our altimeter is chosen to be the nominal direction of the gravitational acceleration at the prescribed hovering point.

For analysis purposes, we assume that the nominal gravitational and centrifugal forces are canceled by open-loop continuous thrusting; thus, the nominally prescribed position is a hovering equilibrium point. We analyze the stability of hovering with the linearized equations of motion and investigate how stability can be enhanced by adding tight closed-loop control along the nominal gravitational direction. With regard to the actual implementation of this control, once the sensing and control direction is chosen, we do not need to specify the open-loop thrust to cancel the gravitational force because the tight controller will do this automatically. We still need to specify the open-loop thrust to cancel the centrifugal force components that are perpendicular to our control direction. When the implementation of such a system is considered, it is clear that implementation errors can arise in several crucial areas, such as the estimated direction

Received 15 May 2001; revision received 30 September 2001; accepted for publication 6 December 2001.

*Visiting Scholar, Department of Aerospace Engineering; also Research Associate, Institute of Space and Astronautical Science, Sagamihara, Kanagawa 229-8510, Japan; sawai@newslan.isas.ac.jp.

†Assistant Professor, Department of Aerospace Engineering; scheeres@umich.edu. Senior Member AIAA.

‡Graduate Student, Department of Aerospace Engineering.

of the gravitational acceleration and the estimated magnitude of the open-loop forces needed to cancel the centripetal acceleration. These issues are also discussed in the paper.

Stability of Hovering over a Uniformly Rotating Body

Stability Analysis for a Point Mass Central Body

First, we consider the case where the central body is a point mass. In this case, stability around the equilibrium point can be investigated analytically. By the use of the coordinates x, y, and z, as in Fig. 1, the equations of motion can be written as

$$\ddot{\boldsymbol{r}} + 2\boldsymbol{\omega} \times \dot{\boldsymbol{r}} + \dot{\boldsymbol{\omega}} \times \boldsymbol{r} + \boldsymbol{\omega} \times (\boldsymbol{\omega} \times \boldsymbol{r}) = \boldsymbol{F}_c + \boldsymbol{F}_g \tag{1}$$

where

$$\boldsymbol{r} \equiv [x, y, z]^T, \qquad \boldsymbol{\omega} \equiv [0, 0, \omega]^T$$

and where

$\boldsymbol{F}_c$ = control acceleration
$\boldsymbol{F}_g$ = gravitational acceleration
ω = angular velocity of central body

Nominally, for an open-loop hovering point, the control acceleration is chosen to equal the sum of the centripetal, tangential, and gravitational accelerations.

We consider perturbations about a nominal hovering point of $\boldsymbol{r}_0 = [x_0, 0, z_0]^T$, leading to a linearized gravitational attraction

$$\boldsymbol{F}_g = \left.\frac{\partial U}{\partial \boldsymbol{r}}\right|_0 + \left[\left.\frac{\partial^2 U}{\partial \boldsymbol{r}^2}\right|_0\right](\boldsymbol{r} - \boldsymbol{r}_0) \tag{2}$$

where $U = \mu/r$. Now, let the coordinates be normalized by the resonance radius, $r_s \equiv (\mu/\omega^2)^{1/3}$, or

$$r_n \equiv \|\boldsymbol{r}_0\|/r_s \tag{3}$$

$$[x_n, z_n] \equiv [x_0/r_s, z_0/r_s] \tag{4}$$

$$[\Delta x, \Delta y, \Delta z]^T \equiv [(x - x_0)/r_s, y/r_s, (z - z_0)/r_s]^T \tag{5}$$

$$\boldsymbol{f}_{c,0} \equiv \boldsymbol{F}_c/r_s \tag{6}$$

and Eq. (1) can be linearized as

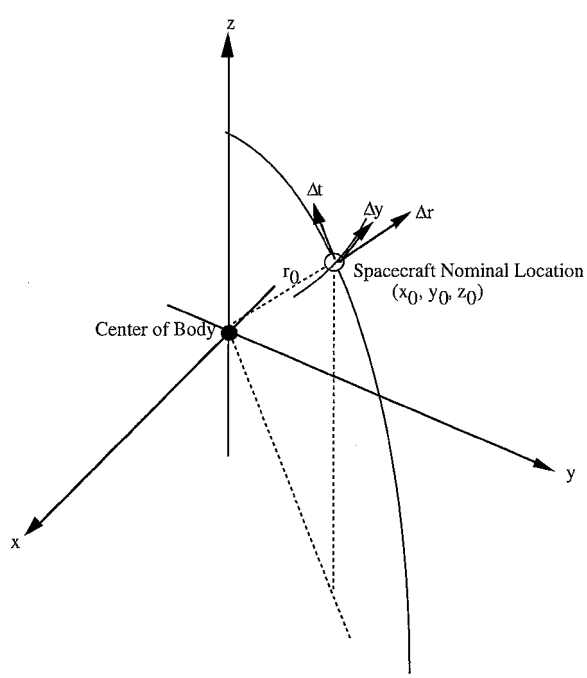

Fig. 1 Body-fixed frame coordinate.

$$\begin{bmatrix}\Delta\ddot{x}\\ \Delta\ddot{y}\\ \Delta\ddot{z}\end{bmatrix} - \begin{bmatrix}0 & 2\omega & 0\\ -2\omega & 0 & 0\\ 0 & 0 & 0\end{bmatrix}\begin{bmatrix}\Delta\dot{x}\\ \Delta\dot{y}\\ \Delta\dot{z}\end{bmatrix} - \left(\begin{bmatrix}\omega^2 & 0 & 0\\ 0 & \omega^2 & 0\\ 0 & 0 & 0\end{bmatrix} + \left[\left.\frac{\partial^2 U}{\partial \boldsymbol{r}^2}\right|_0\right]\right)\begin{bmatrix}\Delta x\\ \Delta y\\ \Delta z\end{bmatrix} = \boldsymbol{f}_{c,0} \tag{7}$$

where

$$\left[\left.\frac{\partial^2 U}{\partial \boldsymbol{r}^2}\right|_0\right] = \omega^2\begin{bmatrix}-\frac{1}{r_n^3} + \frac{3x_n^2}{r_n^5} & 0 & \frac{3x_n z_n}{r_n^5}\\ 0 & -\frac{1}{r_n^3} & 0\\ \frac{3x_n z_n}{r_n^5} & 0 & -\frac{1}{r_n^3} + \frac{3z_n^2}{r_n^5}\end{bmatrix}$$

By the use of the coordinates of Δr, Δy, and Δt, as in Fig. 1, or

$$\begin{bmatrix}\Delta r\\ \Delta y\\ \Delta t\end{bmatrix} \equiv \begin{bmatrix}x_n/r_n & 0 & z_n/r_n\\ 0 & 1 & 0\\ -z_n/r_n & 0 & x_n/r_n\end{bmatrix}\begin{bmatrix}\Delta x\\ \Delta y\\ \Delta z\end{bmatrix} \tag{8}$$

Eq. (7) is transformed to

$$\begin{bmatrix}\Delta\ddot{r}\\ \Delta\ddot{y}\\ \Delta\ddot{t}\end{bmatrix} - 2\omega/r_n\begin{bmatrix}0 & x_n & 0\\ -x_n & 0 & z_n\\ 0 & -z_n & 0\end{bmatrix}\begin{bmatrix}\Delta\dot{r}\\ \Delta\dot{y}\\ \Delta\dot{t}\end{bmatrix} - \omega^2/r_n^2\begin{bmatrix}x_n^2 + 2/r_n & 0 & -x_n z_n\\ 0 & r_n^2 - 1/r_n & 0\\ -x_n z_n & 0 & z_n^2 - 1/r_n\end{bmatrix}\begin{bmatrix}\Delta r\\ \Delta y\\ \Delta t\end{bmatrix} = \begin{bmatrix}f_r\\ f_y\\ f_t\end{bmatrix} \tag{9}$$

where

$$\begin{bmatrix}f_r\\ f_y\\ f_t\end{bmatrix} \equiv \begin{bmatrix}x_n/r_n & 0 & z_n/r_n\\ 0 & 1 & 0\\ -z_n/r_n & 0 & x_n/r_n\end{bmatrix}\boldsymbol{f}_c$$

A tight altitude control using the gravitational direction f_r thrusters will lead to $\Delta r(t) \equiv 0$, reducing Eq. (9) to

$$\begin{bmatrix}\Delta\ddot{y}\\ \Delta\ddot{t}\end{bmatrix} - \frac{2\omega}{r_n}\begin{bmatrix}0 & z_n\\ -z_n & 0\end{bmatrix}\begin{bmatrix}\Delta\dot{y}\\ \Delta\dot{t}\end{bmatrix} - \frac{\omega^2}{r_n^2}\begin{bmatrix}r_n^2 - 1/r_n & 0\\ 0 & z_n^2 - 1/r_n\end{bmatrix}\begin{bmatrix}\Delta y\\ \Delta t\end{bmatrix} = \begin{bmatrix}f_y\\ f_t\end{bmatrix} \tag{10}$$

This equation describes linearized motion with a tight control along the $\boldsymbol{r}_0$ direction. The stability of this controller can be investigated from its characteristic equation

$$s^4 + \omega^2\left\{\frac{2 - r_n^3}{r_n^3} + \frac{3z_n^2}{r_n^2}\right\}s^2 + \omega^4\left(1 - \frac{1}{r_n^3}\right)\left(\frac{z_n^2}{r_n^2} - \frac{1}{r_n^3}\right) = 0 \tag{11}$$

The tightly controlled spacecraft motion is stable if and only if all roots of Eq. (11) have negative or zero real parts with no repeated roots. Note that Eq. (11) corresponds to the zero points of the open-loop spacecraft dynamics, and our tight controller can be considered as the infinity limit of the controller gain. In general, the poles of the infinite gain closed-loop system corresponds to the zero points of the open-loop system. Thus, if Eq. (11) has at least one positive root, it means that the hovering dynamics have at least one unstable zero point, which results in additional complexity for control of the hovering spacecraft.

Generally speaking, if the characteristic equation is

$$s^4 + bs^2 + c = 0 \tag{12}$$

then the stability conditions are

$$b \geq 0 \tag{13}$$

$$c \geq 0 \tag{14}$$

$$b^2 - 4c > 0 \tag{15}$$

In our case, these conditions become

$$\omega^2 \left\{ \frac{2 - r_n^3}{r_n^3} + \frac{3z_n^2}{r_n^2} \right\} \geq 0 \tag{16}$$

$$\omega^4 \left(1 - \frac{1}{r_n^3} \right) \left(\frac{z_n^2}{r_n^2} - \frac{1}{r_n^3} \right) \geq 0 \tag{17}$$

$$\omega^4 \left\{ \frac{2 - r_n^3}{r_n^3} + \frac{3z_n^2}{r_n^2} \right\}^2 - 4\omega^4 \left(1 - \frac{1}{r_n^3} \right) \left(\frac{z_n^2}{r_n^2} - \frac{1}{r_n^3} \right) > 0 \tag{18}$$

or, equivalently,

$$\left(\frac{z_n}{r_n} \right)^2 \geq \frac{-2 + r_n^3}{3r_n^3} \tag{19}$$

$$r_n \leq 1 \qquad \text{or} \qquad \left(\frac{z_n}{r_n} \right)^2 \geq \frac{1}{r_n^3} \tag{20}$$

$$1 < r_n < \sqrt[3]{4} \qquad \text{or}$$

$$\left(\frac{z_n}{r_n} \right)^2 > \frac{5r_n^3 - 8 + \sqrt{\left(5r_n^3 - 8\right)^2 - 9r_n^6}}{9r_n^3} \qquad \text{or}$$

$$\left(\frac{z_n}{r_n} \right)^2 < \frac{5r_n^3 - 8 - \sqrt{\left(5r_n^3 - 8\right)^2 - 9r_n^6}}{9r_n^3} \tag{21}$$

Eqs. (19), (20), and (21) correspond to Eqs. (16), (17), and (18), respectively. The hovering point is stable if and only if Eqs. (19–21) hold, and we note that they hold if $0 < r_n \leq 1$ because then

$$\frac{-2 + r_n^3}{3r_n^3} \leq 0, \qquad \frac{5r_n^3 - 8 + \sqrt{\left(5r_n^3 - 8\right)^2 - 9r_n^6}}{9r_n^3} < 0$$

The stable area of this controller is shown in Fig. 2. Note that the region $r_n < 1$ (i.e., the area within the resonance radius) is stable

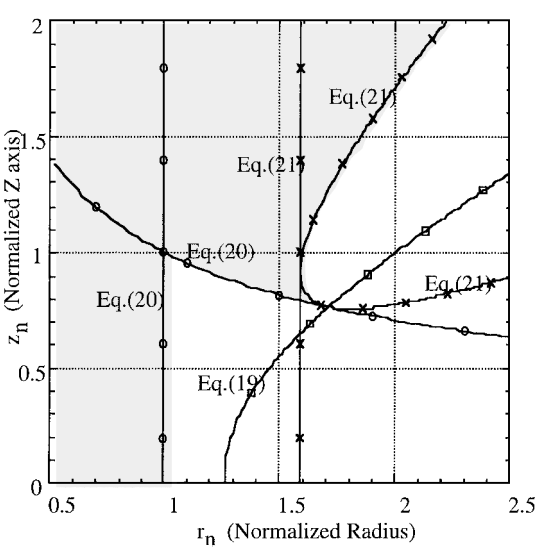

Fig. 2 Stable region of tight altitude control for hovering over a point mass; shaded region corresponds to stable area.

but that regions outside of this limit are not necessarily stable. If the spacecraft position is within the stable area in Fig. 2, hovering can be stabilized with our simple closed-loop controller; conversely, if it is out of this stable area, implementation of hovering requires a more complex controller.

Sufficient Conditions for Stable Hovering Above an Arbitrary Body

The preceding section derived the stable region for hovering over a point mass using a tight controller. This condition can be generalized to an arbitrary gravity field, and the stability of a hovering point can be computed numerically from Eq. (7) using a general gravity field, but the resulting conditions do not lend themselves to analytical description. Instead, we derive a sufficient condition for the stability of our tight controller.

Starting from Eq. (7), let the eigenvalues and eigenvectors of the matrix $[\partial^2 U/\partial \boldsymbol{r}^2]$ be α_1, α_2, and α_3 and $\boldsymbol{v}_1$, $\boldsymbol{v}_2$, and $\boldsymbol{v}_3$, respectively. Because this matrix is symmetric, the eigenvectors are orthogonal to each other and, without loss of generality, we can define the relations

$$\boldsymbol{v}_1 \times \boldsymbol{v}_2 = \boldsymbol{v}_3 \tag{22}$$

$$\boldsymbol{v}_2 \times \boldsymbol{v}_3 = \boldsymbol{v}_1 \tag{23}$$

$$\boldsymbol{v}_3 \times \boldsymbol{v}_1 = \boldsymbol{v}_2 \tag{24}$$

$$\|\boldsymbol{v}_1\| = \|\boldsymbol{v}_2\| = \|\boldsymbol{v}_3\| = 1 \tag{25}$$

When our coordinates are changed,

$$\boldsymbol{x}' = [\boldsymbol{v}_1, \boldsymbol{v}_2, \boldsymbol{v}_3]^{-1} \begin{bmatrix} \Delta x \\ \Delta y \\ \Delta z \end{bmatrix} = \begin{bmatrix} \boldsymbol{v}_1^T \\ \boldsymbol{v}_2^T \\ \boldsymbol{v}_3^T \end{bmatrix} \begin{bmatrix} \Delta x \\ \Delta y \\ \Delta z \end{bmatrix} \tag{26}$$

Eq. (7) becomes

$$\ddot{\boldsymbol{x}}' - 2\omega \begin{bmatrix} 0 & -v_{3z} & v_{2z} \\ v_{3z} & 0 & -v_{1z} \\ -v_{2z} & v_{1z} & 0 \end{bmatrix} \dot{\boldsymbol{x}}' - \left\{ \begin{bmatrix} \alpha_1 + \omega^2 & 0 & 0 \\ 0 & \alpha_2 + \omega^2 & 0 \\ 0 & 0 & \alpha_3 + \omega^2 \end{bmatrix} - \omega^2 \begin{bmatrix} v_{1z} \\ v_{2z} \\ v_{3z} \end{bmatrix} \times [v_{1z}, v_{2z}, v_{3z}] \right\} \boldsymbol{x}' = \boldsymbol{f}' \tag{27}$$

For most cases, one of the eigenvectors ($\boldsymbol{v}_3$, for example) is almost aligned with the gravitational attraction, and two of the eigenvalues (α_1 and α_2) are stable, that is, have negative values. The vectors $\boldsymbol{v}_1$ and $\boldsymbol{v}_2$ are approximately tangent to the surface of constant gravity potential, and the vector $\boldsymbol{v}_3$ is approximately aligned with the direction of the gravitational attraction. This is exactly true if the central body is a point mass. Here, $\boldsymbol{v}_3$ is defined as the quasi-gravity direction. When we adopt our tight controller in the $\boldsymbol{v}_3$ direction (both observation and thrusting), Eq. (27) will reduce to

$$\ddot{\boldsymbol{x}}' - 2\omega \begin{bmatrix} 0 & -v_{3z} \\ v_{3z} & 0 \end{bmatrix} \dot{\boldsymbol{x}}' - \left\{ \begin{bmatrix} \alpha_1 + \omega^2 & 0 \\ 0 & \alpha_2 + \omega^2 \end{bmatrix} - \omega^2 \begin{bmatrix} v_{1z} \\ v_{2z} \end{bmatrix} [v_{1z}, v_{2z}] \right\} \boldsymbol{x}' = \boldsymbol{f}' \tag{28}$$

with a characteristic equation of the form

$$s^4 + bs^2 + c = 0 \tag{29}$$

where

$$b = 4\omega^2 v_{3z}^2 - k_1 - k_2 \tag{30}$$

$$c = -\omega^4 v_{1z}^2 v_{2z}^2 + k_1 k_2 \tag{31}$$

$$k_1 = \alpha_1 + \omega^2 - v_{1z}^2\omega^2 \tag{32}$$

$$k_2 = \alpha_2 + \omega^2 - v_{2z}^2\omega^2 \tag{33}$$

The stability conditions for the tight controller are the same as in Eqs. (13–15), or

$$3\omega^2 v_{3z}^2 + \omega^2 - \left(\alpha_1 + \omega^2\right) - \left(\alpha_2 + \omega^2\right) \geq 0 \tag{34}$$

$$\left(\alpha_1 + \omega^2\right)\left(\alpha_2 + \omega^2\right) - \omega^2 v_{1z}^2\left(\alpha_2 + \omega^2\right) - \omega^2 v_{2z}^2\left(\alpha_1 + \omega^2\right) \geq 0 \tag{35}$$

$$\left(\alpha_1 - \alpha_2 - \omega^2\right)^2 + 3\omega^4 v_{3z}^2\left(v_{3z}^2 + 2\right) - 8\omega^2 v_{3z}^2\left\{\left(\alpha_1 + \omega^2\right) + \left(\alpha_2 + \omega^2\right)\right\} > 0 \tag{36}$$

We can verifty that Eqs. (34–36) will hold if

$$\alpha_1 + \omega^2 \leq 0 \tag{37}$$

$$\alpha_2 + \omega^2 \leq 0 \tag{38}$$

Equations (37) and (38) are the sufficient conditions for the stability of the tight control along the quasi-gravity direction. In the case of a sphere, these sufficiency conditions reduce to $r/r_s \leq 1$, which is what we had found earlier. In the general case, these values of α are easily computed at an arbitrary point from the second derivative of the gravity potential.

Numerical Computation of the Stable Area

To validate our sufficient condition, a number of numerical checks were conducted. Here, the central body is assumed to be an ellipsoid (Figs. 3 and 4) or the realistic shape of asteroid Castalia[4] (Figs. 5 and 6). Rotation periods of 4.07 h (Castalia's estimated rotation period) and 10 h (for comparison) were investigated. Figures 2–6 show that similar stable regions exist for the sphere, ellipsoid, and Castalia, a similarity that degrades at faster rotation speeds. Figures 3–6 also show the area where the sufficient condition, derived from our earlier discussion, is satisfied. We note that the sufficient areas coincide closely with the actual stable areas near the asteroid surface.

Even with a perfectly applied tight controller, some residual motions will exist due to errors in the initial placement of the spacecraft. The frequencies of these residual modes are of interest because, if they are too fast, the hovering trajectory can easily become unstable with a small time lag in the controller. In contrast, if they are too slow, the hovering position deviations can become large with only small initial velocity errors. From our numerical analysis, we find that hovering near the stability limit is not robust against velocity errors due to the slow residual modes in this region, but becomes more robust as the hovering point approaches the central body.

Summary

In this section, the stability of hovering under tight control has been discussed. The stability conditions are deduced explicitly for a point mass, where we find hovering to be stable for the region inside

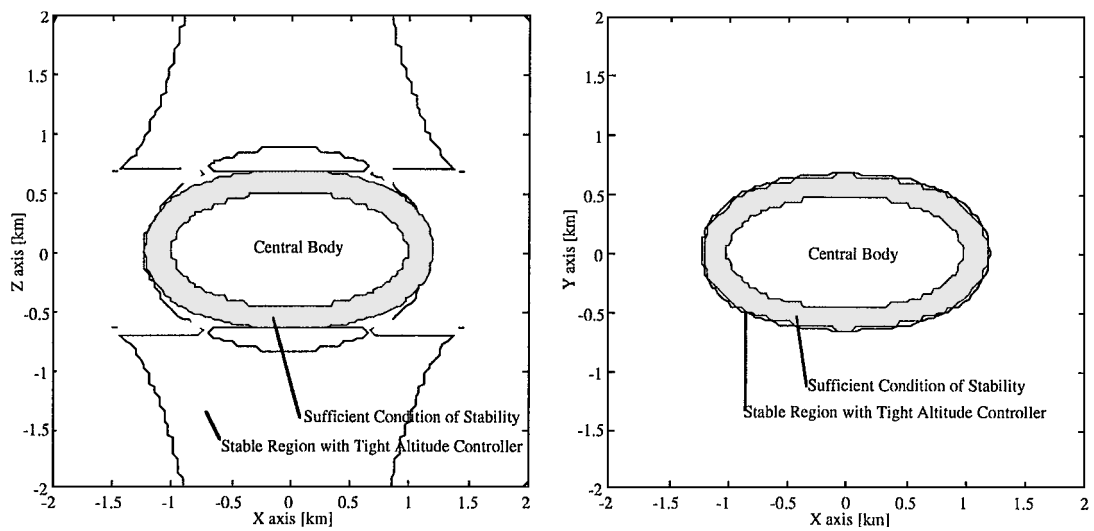

Fig. 3 Stable region of tight altitude control for hovering over an ellipsoid with a rotation period of 4.07 h (rotation about *Z* axis).

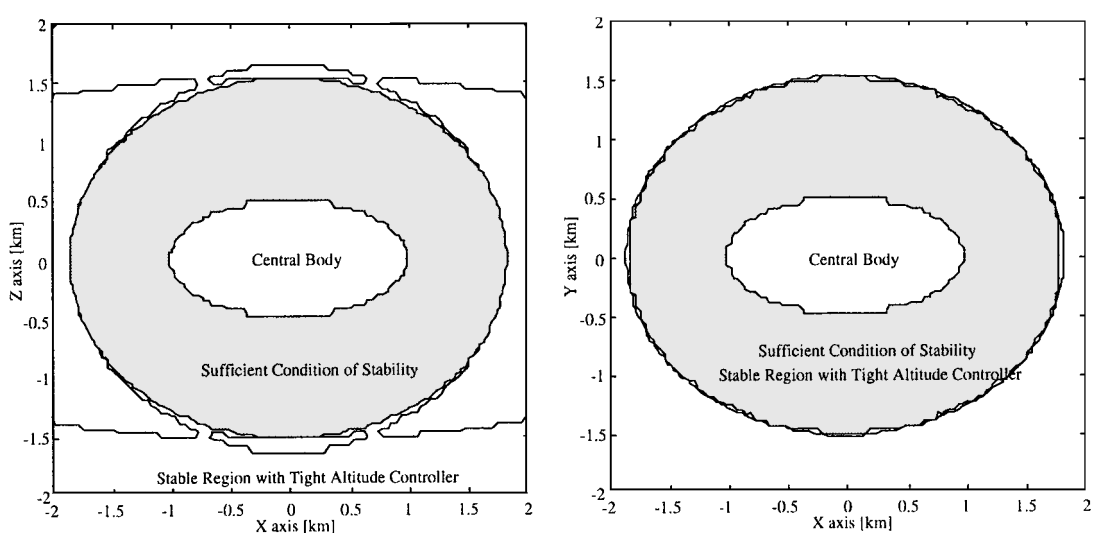

Fig. 4 Stable region of tight altitude control for hovering over an ellipsoid with a rotation period of 10.0 h (rotation about *Z* axis).

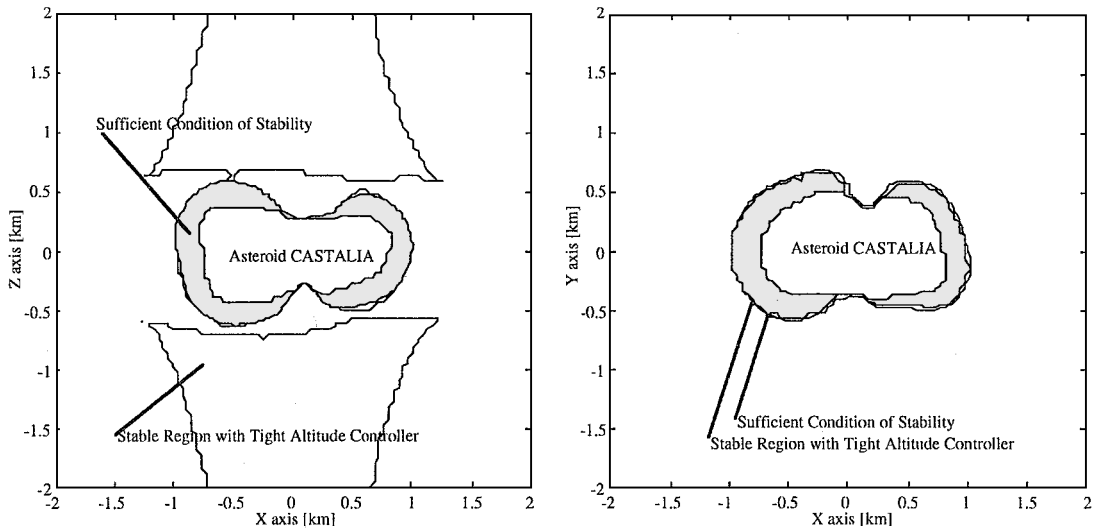

Fig. 5 Stable region of tight altitude control for hovering over Castalia with a rotation period of 4.07 h (rotation about *Z* axis).

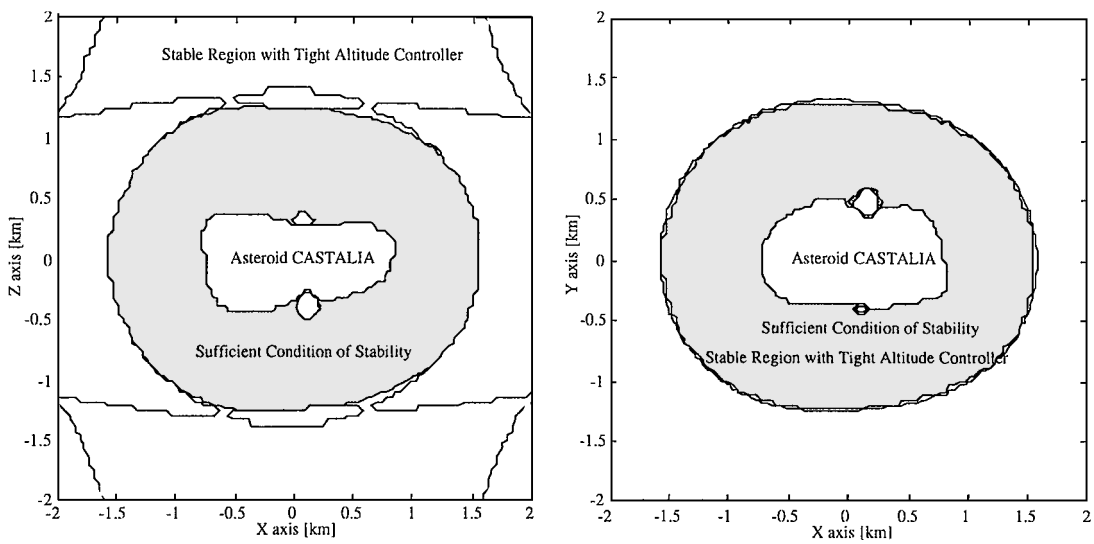

Fig. 6 Stable region of tight altitude control for hovering over Castalia with a rotation period of 10.0 h (rotation about *Z* axis).

the resonance radius. For a general mass distribution, analytical results are not possible. Thus, reliance is made on numerical checks of stability. We are, however, able to derive a simpler sufficient condition in this case that agrees well with the full stability conditions. The maximum altitude for the stable hovering can be defined as the resonance radius, or the radius at which Eqs. (37) and (38) hold.

Sensitivity of the Control to Errors

As noted earlier, the ideal implementation of our control and the practical implementation of it will have significant differences. To evaluate whether our theoretical approach to computing the stability of motion is reasonable, we evaluate the sensitivity of our control to several different error sources.

Sensitivity to Errors in the Control Direction

For an actual spacecraft, some discrepancies will exist between the open-loop thrust that cancels the centrifugal force, the estimated direction of gravitational attraction (and, hence, the sensing and control direction), and the hovering altitude. Ideally, the hovering equilibrium point will be where these points coincide with their estimated values, but, in general, there will be inconsistencies among them, and there will be no single point where they coincide exactly with their estimated values. Thus, the actual equilibrium point will be a compromise among these values. For example, if the estimated direction of the gravitational acceleration has some error, the actual equilibrium point will shift to a point where the vector sum of the erroneous direction, the gravity acceleration, and the deviation of the centrifugal force sum to zero.

In this discussion, we wish to place constraints on how large of a shift in the actual hovering point will occur due to these errors. We will use the linearized equations

$$\ddot{\boldsymbol{x}} - 2\omega \begin{bmatrix} 0 & -1 & 0 \\ 1 & 0 & 0 \\ 0 & 0 & 0 \end{bmatrix} \dot{\boldsymbol{x}} - \left\{ \begin{bmatrix} \omega^2 & 0 & 0 \\ 0 & \omega^2 & 0 \\ 0 & 0 & 0 \end{bmatrix} + \left[\frac{\partial^2 U}{\partial \boldsymbol{r}^2} \right] \right\} \boldsymbol{x} = \boldsymbol{f}_c \tag{39}$$

$$\boldsymbol{f}_c = \boldsymbol{f}_{c,g} + \boldsymbol{f}_{c,c} \tag{40}$$

where $\boldsymbol{x}$ is the deviation of the spacecraft from the nominal hovering point, $\boldsymbol{f}_{c,g}$ is the closed-loop control force, and $\boldsymbol{f}_{c,c}$ is the force that cancels the centrifugal force, added in an open-loop manner. The nominal position $\boldsymbol{x} = 0$ is defined as the point where the gravity attraction is aligned with the control force $\boldsymbol{f}_{c,g}$ and where the hovering altitude equals the commanded value.

We assume that $\boldsymbol{f}_{c,c}$ is the force balanced with the actual centrifugal force at a position $\boldsymbol{x}_c$, or, in other words, $\boldsymbol{x}_c$ is the vector from $\boldsymbol{x} = 0$ to the point where the centrifugal force and the open-loop cancellation force balance. Ideally, $\boldsymbol{x}_c = 0$, but, due to errors, $\boldsymbol{x}_c \neq 0$, in general.

For this case, Eq. (39) becomes

$$\ddot{\boldsymbol{x}} - 2\omega \begin{bmatrix} 0 & -1 & 0 \\ 1 & 0 & 0 \\ 0 & 0 & 0 \end{bmatrix} \dot{\boldsymbol{x}} + \left\{ \begin{bmatrix} \omega^2 & 0 & 0 \\ 0 & \omega^2 & 0 \\ 0 & 0 & 0 \end{bmatrix} + \begin{bmatrix} \dfrac{\partial^2 U}{\partial \boldsymbol{r}^2} \end{bmatrix} \right\} \boldsymbol{x}$$

$$= \boldsymbol{f}_{c,g} + \begin{bmatrix} \omega^2 & 0 & 0 \\ 0 & \omega^2 & 0 \\ 0 & 0 & 0 \end{bmatrix} \boldsymbol{x}_c \tag{41}$$

At the equilibrium point, $\ddot{\boldsymbol{x}}$ and $\dot{\boldsymbol{x}}$ are equal to zero, so that

$$\begin{bmatrix} \dfrac{\partial^2 U}{\partial \boldsymbol{r}^2} \end{bmatrix} \boldsymbol{x} + \begin{bmatrix} \omega^2 & 0 & 0 \\ 0 & \omega^2 & 0 \\ 0 & 0 & 0 \end{bmatrix} (\boldsymbol{x} - \boldsymbol{x}_c) = \boldsymbol{f}_{c,g} \tag{42}$$

or

$$A\boldsymbol{x} = B\boldsymbol{x}_c + f\boldsymbol{v}_g \tag{43}$$

where

$$A \equiv \begin{bmatrix} \dfrac{\partial^2 U}{\partial \boldsymbol{r}^2} \end{bmatrix} + \begin{bmatrix} \omega^2 & 0 & 0 \\ 0 & \omega^2 & 0 \\ 0 & 0 & 0 \end{bmatrix} \tag{44}$$

$$B \equiv \begin{bmatrix} \omega^2 & 0 & 0 \\ 0 & \omega^2 & 0 \\ 0 & 0 & 0 \end{bmatrix} \tag{45}$$

$$\boldsymbol{f}_{c,g} \equiv f\boldsymbol{v}_g \tag{46}$$

$$\|\boldsymbol{v}_g\| = 1 \tag{47}$$

holds. Note that $\boldsymbol{v}_g$ points along the estimated gravitational attraction and, thus, keeps altitude constant along this direction. At the equilibrium point, this control force will also be constant.

The matrix A will not be singular, in general, and so Eq. (43) can be rewritten as

$$\boldsymbol{x} = A^{-1}B\boldsymbol{x}_c + fA^{-1}\boldsymbol{v}_g \tag{48}$$

The control force $\boldsymbol{f}_{c,g}$ will keep the altitude as commanded, meaning that $\boldsymbol{v}_g \cdot \boldsymbol{x} = 0$ will hold; thus,

$$0 = \boldsymbol{v}_g^T A^{-1} B\boldsymbol{x}_c + f\boldsymbol{v}_g^T A^{-1}\boldsymbol{v}_g \tag{49}$$

and we can solve for the control force as

$$f = -\left(1 \Big/ \boldsymbol{v}_g^T A^{-1}\boldsymbol{v}_g\right)\boldsymbol{v}_g^T A^{-1} B\boldsymbol{x}_c \tag{50}$$

From Eq. (48),

$$\boldsymbol{v}^T\boldsymbol{x} = \boldsymbol{v}^T A^{-1} B\boldsymbol{x}_c + f\boldsymbol{v}^T A^{-1}\boldsymbol{v}_g \tag{51}$$

$$= \boldsymbol{v}^T \left\{ I - \frac{A^{-1}\boldsymbol{v}_g\boldsymbol{v}_g^T}{\boldsymbol{v}_g^T A^{-1}\boldsymbol{v}_g} \right\} A^{-1} B\boldsymbol{x}_c \tag{52}$$

Because this equation holds for an arbitrary vector $\boldsymbol{v}$,

$$\boldsymbol{x} = M\boldsymbol{x}_c \tag{53}$$

$$M = \left\{ I - \frac{A^{-1}\boldsymbol{v}_g\boldsymbol{v}_g^T}{\boldsymbol{v}_g^T A^{-1}\boldsymbol{v}_g} \right\} A^{-1} B \tag{54}$$

This equation relates the sensitivity of the equilibrium point $\boldsymbol{x}$ with respect to $\boldsymbol{x}_c$. The maximum singular value of matrix M must be small for the hovering equilibrium points to be insensitive to these errors.

The eigenvectors of M have some interesting characteristics. For example, because

$$\boldsymbol{v}_g^T M = \left\{ \boldsymbol{v}_g^T - \frac{\boldsymbol{v}_g^T A^{-1}\boldsymbol{v}_g\boldsymbol{v}_g^T}{\boldsymbol{v}_g^T A^{-1}\boldsymbol{v}_g} \right\} A^{-1} B = \boldsymbol{0} \tag{55}$$

the eigenvectors of nonzero eigenvalues must be perpendicular to the vector $\boldsymbol{v}_g$. Also, because

$$B \begin{bmatrix} 0 \\ 0 \\ 1 \end{bmatrix} = \boldsymbol{0} \tag{56}$$

the z axis (equal to spin axis) direction is one of the eigenvectors with a zero eigenvalue. From numerical checks of the eigenvalues of M, it is found that the equilibrium points become insensitive to these errors as the hovering altitude decreases.

Sensitivity to Other Factors

Numerical simulations of hovering trajectories were carried out to examine the sensitivity of the stable hovering points due to realistic control implementation errors. Most state-of-the-art spacecraft have impulsive thrusters instead of continuous ones, and so the assumption of continuous thrusting adopted here will not hold for most spacecraft. This implies that we should investigate the error due to this approximation. The controller adopted in our simulations is designed to be a realistic model of a tight controller along the estimated direction of gravitational acceleration. Thus, centrifugal forces are canceled periodically with an impulsive force, and we simulate the tight altitude control with a deadband controller where the altitude is held within an interval about the prescribed value by firing control thrusters whenever this deadband is violated. Our control logic checks whether the spacecraft has violated the deadband every second and applies a small impulse to the spacecraft until the criterion is satisfied. Additionally, no open-loop logic is used to cancel the nominal gravitational attraction because the necessary quasi-continuous force to null out gravitational force is obtained from the closed-loop control.

Simulations were carried out to evaluate the robustness of hovering as a function of position. The central body was assumed to be an ellipsoid of dimensions $0.5 \times 0.5 \times 1.0$ km with a rotation period of 10 h. Two hovering positions were selected, both within the formal stability area, to show the difference between hovering close to, and further from, the central body. The close hovering point was chosen to lie at (0.65, 0.00, and 0.50 km) and the far hovering point was chosen to lie at (1.65, 0.00, and 0.50 km).

The combination of parameters used in our simulations is summarized in Table 1. Case 1 stands for the nominal case. In case 2, the period between centrifugal force cancellations is increased. Because the rotation period of the body is 10 h, it rotates 72 deg between each cancellation in this case. Case 3 represents the influence of a large deadband width, one comparable to the central body size. Cases 4 and 5 represent errors in the initial velocity of the hovering spacecraft in the body-fixed frame (ideally equal to zero). Cases 6 and 7 show the effects of errors in the gravitational direction.

All of the simulation cases were stable for the close hovering position. For the far hovering position, only cases 1–3 were stable, whereas cases 4–7 were unstable. This suggests that the hovering trajectory is robust with respect to the frequency of the centrifugal force application and the width of the dead band. If the hovering position is near the resonance radius, stability becomes sensitive to velocity errors because the residual modes have low frequencies that result in large amplitude oscillations. Furthermore, hovering is not as robust with respect to the gravitational direction error if the hovering position is located near the resonance radius.

Table 1 Combination of parameters used for numerical simulations

Case number	Centrifugal force cancellation period, min	Dead band width, m	Initial velocity error, cm/s	Gravity direction error, deg
1	10	1.0	0.0	0.0
2	120	1.0	0.0	0.0
3	10	100	0.0	0.0
4	10	1.0	1.0	0.0
5	10	1.0	10.0	0.0
6	10	1.0	0.0	0.4
7	10	1.0	0.0	8.4

Stability of Hovering over a Nonuniformly Rotating Body

In the preceding section, the central body was assumed to be a uniformly rotating body. However, not all small bodies rotate uniformly (cf. Harris[5]). Thus, an important extension to this research is to investigate how the nonuniform rotation of a body may affect the stability of hovering. The equations of motion for such a situation can be expressed using Eq. (1) by taking ω as the time-varying angular velocity of the body.

Angular Velocity of Nutating Body

In general, the angular velocity of a rotating body satisfies the Euler equations:

$$\boldsymbol{I}\dot{\boldsymbol{\omega}} + \boldsymbol{\omega} \times \boldsymbol{I}\boldsymbol{\omega} = 0 \tag{57}$$

or, equivalently,

$$\boldsymbol{I}_x\dot{\omega}_x + (\boldsymbol{I}_z - \boldsymbol{I}_y)\omega_y\omega_z = 0 \tag{58}$$

$$\boldsymbol{I}_y\dot{\omega}_y + (\boldsymbol{I}_x - \boldsymbol{I}_z)\omega_z\omega_x = 0 \tag{59}$$

$$\boldsymbol{I}_z\dot{\omega}_z + (\boldsymbol{I}_y - \boldsymbol{I}_x)\omega_x\omega_y = 0 \tag{60}$$

where $\boldsymbol{I}_x$, $\boldsymbol{I}_y$, and $\boldsymbol{I}_z$ are the moments of inertia of the central body and $\boldsymbol{\omega} \equiv [\omega_x, \omega_y, \omega_z]^T$ is the angular velocity of the body (in body-fixed frame).

For simplicity, we assume an axially symmetric inertia tensor,

$$\boldsymbol{I}_x = \boldsymbol{I}_y \neq \boldsymbol{I}_z \tag{61}$$

Then the general solution to Eq. (57) becomes

$$\omega_x = \omega_0 \sin\theta \cos(\omega_n t) \tag{62}$$

$$\omega_y = \omega_0 \sin\theta \sin(\omega_n t) \tag{63}$$

$$\omega_z = \omega_0 \cos\theta \tag{64}$$

$$\omega_n = \sigma\omega_0 \cos\theta \tag{65}$$

$$\sigma \equiv (\boldsymbol{I}_z - \boldsymbol{I}_x)/\boldsymbol{I}_x$$

angular velocity. The angular momentum vector in the body-fixed frame becomes

$$\boldsymbol{H} = \begin{bmatrix} \boldsymbol{I}_x\omega_0 \sin\theta \cos(\omega_n t) \\ \boldsymbol{I}_x\omega_0 \sin\theta \sin(\omega_n t) \\ \boldsymbol{I}_z\omega_0 \cos\theta \end{bmatrix} \tag{66}$$

When θ_H is defined as the angle between the z axis and the angular momentum vector, the following relations hold:

$$\cos\theta_H = \frac{(\sigma+1)\cos\theta}{\sqrt{(\sigma+1)^2\cos^2\theta + \sin^2\theta}} \tag{67}$$

$$\cos(\theta_H - \theta) = \frac{(\sigma+1)\cos^2\theta + \sin^2\theta}{\sqrt{(\sigma+1)^2\cos^2\theta + \sin^2\theta}} \tag{68}$$

Substituting Eqs. (62–65) into Eq. (1) yields

$$\ddot{\boldsymbol{r}} + 2\omega_0 \begin{bmatrix} 0 & -\cos\theta & \sin\theta\sin(\omega_n t) \\ \cos\theta & 0 & -\sin\theta\cos(\omega_n t) \\ -\sin\theta\sin(\omega_n t) & \sin\theta\cos(\omega_n t) & 0 \end{bmatrix} \dot{\boldsymbol{r}}$$

$$+ \omega_0 \begin{bmatrix} -\sin^2\theta\sin^2(\omega_n t) - \cos^2\theta & \sin^2\theta\sin(\omega_n t)\cos(\omega_n t) & \sin\theta\cos\theta\cos(\omega_n t) \\ \sin^2\theta\sin(\omega_n t)\cos(\omega_n t) & -\sin^2\theta\cos^2(\omega_n t) - \cos^2\theta & \sin\theta\cos\theta\sin(\omega_n t) \\ \sin\theta\cos\theta\cos(\omega_n t) & \sin\theta\cos\theta\sin(\omega_n t) & -\sin^2\theta \end{bmatrix} \boldsymbol{r} = \boldsymbol{F}_g + \boldsymbol{F}_c \tag{69}$$

where $\boldsymbol{r} = [x, y, z]^T$.

Point Mass Gravity Field Case

First assume a point mass gravitational field. In general, for a point mass, the relation $I_x = I_y = I_z$ will hold, and rotation will be uniform about any axis. Thus, the assumption adopted here is not entirely consistent, but is useful for understanding the nature of stability of hovering over a nonuniformly rotating body.

When the coordinates are changed as depicted in Fig. 1, the gravitational attraction in this coordinate frame becomes

$$\boldsymbol{F}_g = \boldsymbol{F}_{g,0} + \frac{\mu}{r_0^3}\begin{bmatrix} 2 & 0 & 0 \\ 0 & -1 & 0 \\ 0 & 0 & -1 \end{bmatrix} \boldsymbol{r}_2 \tag{70}$$

where $\boldsymbol{r}_2 = [\Delta r, \Delta y, \Delta t]^t$ and $r_0 = \sqrt{(x_0^2 + y_0^2 + z_0^2)}$.

Assume that a tight controller is applied again in the radial direction and that distance is normlized by the resonance radius, $r_s \equiv (\mu/\omega_0^2)^{1/3}$. Then the residual motion will be described as

$$\ddot{\boldsymbol{r}}_3 + \frac{2\omega_0}{r_n}\left\{x_n \sin\theta\cos(\omega_n t) + z_n\cos\theta\right\}\begin{bmatrix} 0 & -1 \\ 1 & 0 \end{bmatrix}\dot{\boldsymbol{r}}_3 + \frac{-x_n\omega_0\omega_n \sin\theta\sin(\omega_n t)}{r_n}\begin{bmatrix} 0 & -1 \\ 1 & 0 \end{bmatrix}\boldsymbol{r}_3 + \omega_0^2$$

$$\times \begin{bmatrix} -1 - \sin^2\theta\cos^2(\omega_n t) + \dfrac{1}{r_n^3} & \sin\theta\sin(\omega_n t)\left\{\dfrac{x_n}{r_n}\cos\theta - \dfrac{z_n}{r_n}\sin\theta\cos(\omega_n t)\right\} \\ \sin\theta\sin(\omega_n t)\left\{\dfrac{x_n}{r_n}\cos\theta - \dfrac{z_n}{r_n}\sin\theta\cos(\omega_n t)\right\} & -\dfrac{x_n^2}{r_n^2}\sin^2\theta - \dfrac{z_n^2}{r_n^2}\left\{\cos^2\theta + \sin^2\theta\sin^2(\omega_n t)\right\} - 2\dfrac{x_n z_n}{r_n^2}\sin\theta\cos\theta\cos(\omega_n t) + \dfrac{1}{r_n^3} \end{bmatrix} \boldsymbol{r}_3 = 0 \tag{71}$$

where ω_0 and θ are constant.

Note that ω_0 is the magnitude of the angular velocity and θ is the angle between the z axis (body-fixed axis of symmetry) and the

where $\boldsymbol{r}_3 = [\Delta y/r_s, \Delta t/r_s]^t$.

Because Eq. (71) is linear and time periodic, the stability of solutions to this equation can be investigated using Floquet theory

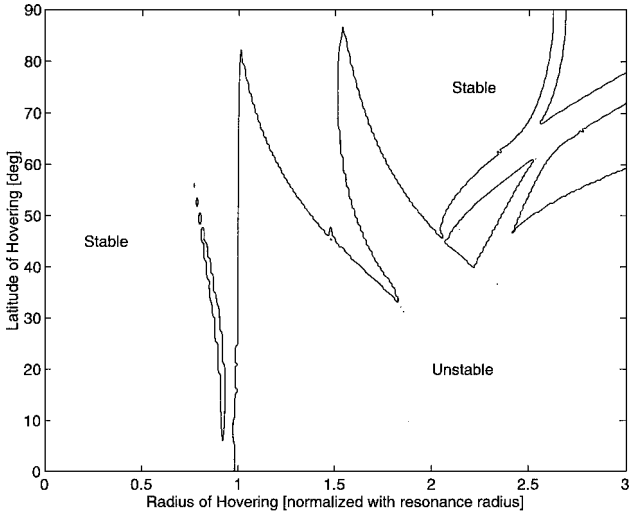

Fig. 7 Stable region of hovering over a nutating point mass (nutation angle 15 deg, $I_z/I_x = 0.4$).

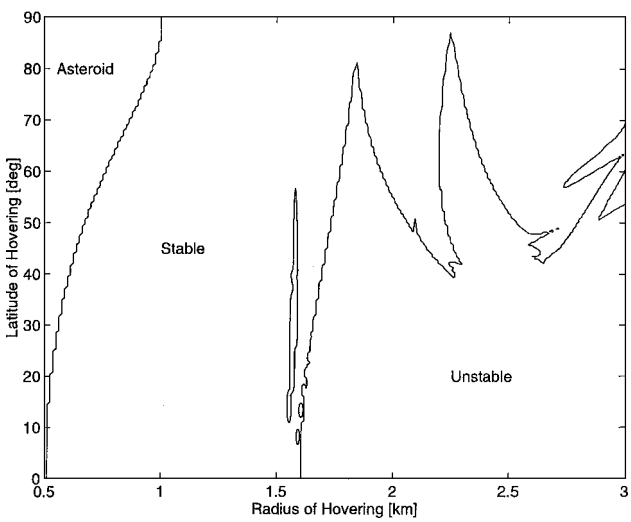

Fig. 8 Stable region of hovering over an ellipsoid in nonprincipal axis rotation (nutation angle 15 deg, $I_z/I_x = 0.4$).

(see Ref. 6). Hovering is stable if and only if the eigenvalues of the state transition matrix taken over one period are all complex with unity magnitude. The stable hovering regions over a nonuniformly rotating point mass with a specific nutation angle and inertia ratio are shown in Fig. 7. We see that the stable regions are similar to the uniformly rotating case, and that the region near the central body remains stable. This can also be seen for non-point mass gravity cases, where Fig. 8 shows the stability diagram for an ellipsoidal body of dimensions $0.5 \times 0.5 \times 1.0$ km, constant density of 2.0 g/cm^3, and a specified nutation angle. Thus, for hovering over a nonuniformly rotating body, we can verify that there exist stable regions close to the central body, analogous to the uniformly rotating case.

Translational Motion over Bodies

Hovering opens new possibilities for the scientific investigation of a body. However, hovering over a single point will not produce the type of global information that is desired. Thus, an important consideration will be to model the dynamics and stability of translational spacecraft motions that occur while the hovering control loop is enabled.

Translational Motion over a Point Mass

Again, the case of a point mass is first treated for simplicity. In this case, the stability of translational motion can be reduced to the stability of hovering at a fixed point.

The gravity potential and attraction are again

$$U = \frac{\mu}{|\boldsymbol{r}|} \tag{72}$$

$$\boldsymbol{F}_g = \frac{\partial U}{\partial \boldsymbol{r}} = -\frac{\mu}{|\boldsymbol{r}|^3}\boldsymbol{r} \tag{73}$$

where μ denotes the gravity constant. For small deviations from the nominal point, we use the approximation

$$\boldsymbol{F}_g - \boldsymbol{F}_{g,0} \approx \left.\frac{\partial^2 U}{\partial \boldsymbol{r}^2}\right|_0 \Delta\boldsymbol{r} \tag{74}$$

where $\boldsymbol{F}_{g,0}$ denotes the gravitational attraction that occurs if the spacecraft translates exactly on the prescribed path. When this is substituted into Eq. (1) and linearized, deviations from the prescribed path obey the equations

$$\Delta\ddot{\boldsymbol{r}} + 2\boldsymbol{\omega} \times \Delta\dot{\boldsymbol{r}} + \dot{\boldsymbol{\omega}} \times \Delta\boldsymbol{r} + \boldsymbol{\omega} \times (\boldsymbol{\omega} \times \Delta\boldsymbol{r}) = \left.\frac{\partial^2 U}{\partial \boldsymbol{r}^2}\right|_0 \Delta\boldsymbol{r} + \boldsymbol{F}_c \tag{75}$$

Because of spherical symmetry of a point mass gravity field, this equation holds for all $\boldsymbol{\omega}$. Thus, it is possible to set $\boldsymbol{\omega}$ to an arbitrary angular velocity with respect to the inertial frame to generate a constant altitude translational motion around the body. In practice, one would define the great circle between the desired locations on the asteroid surface, the normal to this plane $\hat{\boldsymbol{u}}$, the angle subtended in this plane θ, and the time of the transfer τ to compute the body-relative rotational velocity $\boldsymbol{\omega}_\theta = (\theta/\tau)\hat{\boldsymbol{u}}$. The total angular velocity to be used in Eq. (75) is then the sum of the actual body angular rate and the relative translational rate just defined. Because of the symmetry of the point mass gravity field, Eq. (75) is identical to the hovering equation over a uniformly rotating point mass with angular velocity $\boldsymbol{\omega}$. Thus, if the closed-loop control $\boldsymbol{F}_c$ is added to keep the altitude constant, the translational motion is stable when the spacecraft altitude is less than r_s, where

$$r_s \equiv (\mu/|\boldsymbol{\omega}|^2)^{\frac{1}{3}} \tag{76}$$

and where $|\boldsymbol{\omega}|$ is now the magnitude of the body's angular velocity vector plus $\boldsymbol{\omega}_\theta$.

To enhance stability and robustness, r_s can be enlarged by reducing the total angular velocity $\boldsymbol{\omega}$ relative to inertial space. Thus, when possible, the direction of translational motion should be taken in a sense opposite to the body's rotation because this results in the reduction of the translational angular velocity $\boldsymbol{\omega}$ in the inertial frame. From this, we also see that a fast translation in the direction of small-body rotation can destabilize the control.

Translational Motion over Arbitrary Bodies

Translational motion described in the preceding section is motion at a constant altitude. This can be generalized to translational motion along a contour line of constant gravitational potential. Then, for an arbitrarily shaped, uniformly rotating body, the spacecraft translates along a line on the constant gravity potential surface where the altitude of the path is determined by its latitude and the longitude in the body-fixed space. Other approaches to specifing translational motion are possible; however, we have chosen this one for definiteness in our simulations. With an ideal open-loop cancellation of the force, the equations of motion of the spacecraft are similar in form to Eq. (75), but now the force potential U is arbitrary and evaluated along the path of the spacecraft, $\boldsymbol{\omega}$ is just the angular velocity of the body rotation again, and the open-loop control also accounts for Coriolis accelerations that arise due to the motion of the hovering spacecraft. If the spacecraft has an altimeter onboard, and if a controller is present that forces the altimeter output to follow the prescribed altitude profile, the control law becomes

$$\Delta\boldsymbol{r} \cdot \left.\frac{\partial U}{\partial \boldsymbol{r}}\right|_0 = 0 \tag{77}$$

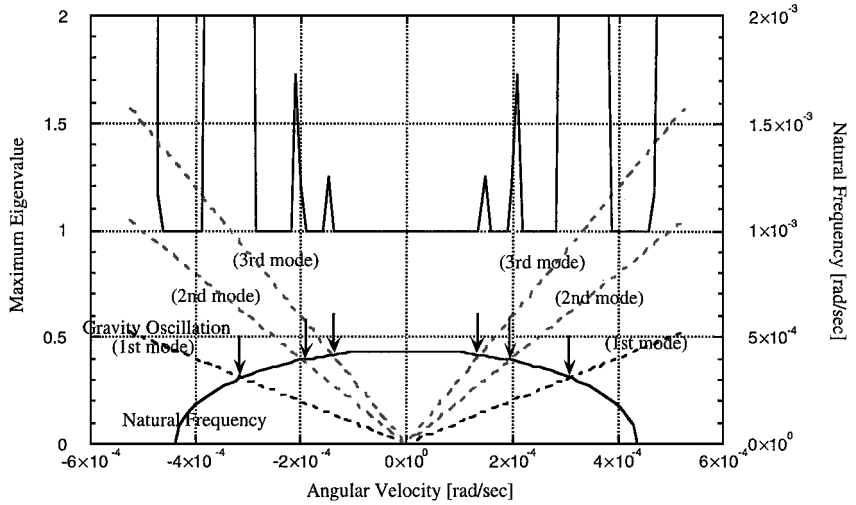

Fig. 9 Stability of transition over a nonrotating ellipsoid.

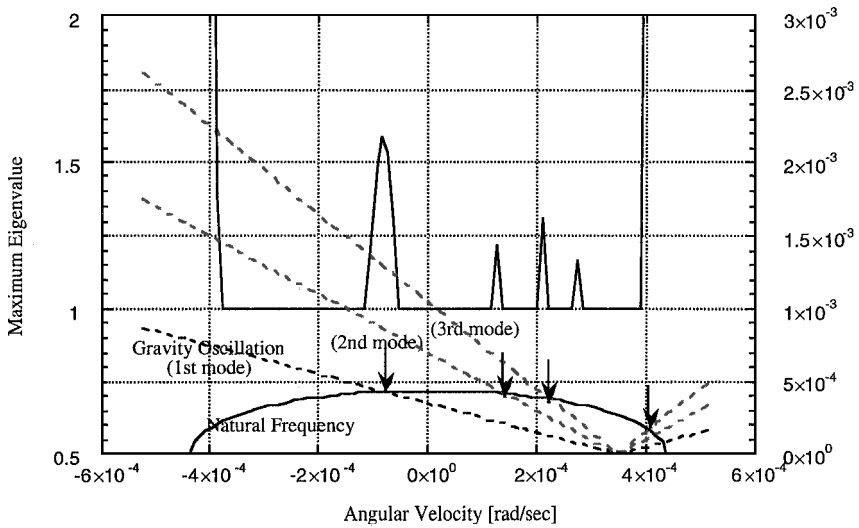

Fig. 10 Stability of transition over a rotating ellipsoid with period of 5 h.

The resulting trajectory is a time-varying trajectory in the body-fixed frame and can be analyzed using linear systems theory.

In Fig. 9, the stability of a translation maneuver as a function of transfer speed is shown for the case of a nonrotating ellipsoid (with the same dimensions and density used earlier). The vertical axis shows the maximum eigenvalue of the transition matrix over one period. If its value is larger than 1.0, the transition is unstable. The horizontal axis shows the transition angular velocity. Also plotted in Fig. 9 is the natural frequency of the residual motion, which is the oscillation frequency of a stabilized hovering spacecraft in the body-fixed frame. The dotted lines represent integral multiples of the angular velocity of the body in the spacecraft fixed frame. Note that the translation maneuvers become unstable if the natural frequency of the spacecraft motion is synchronous with these angular velocities. For the case of a nonrotating body, we see that there is a symmetry between translation motions in the positive and negative sense. In Fig. 10, we show the stability diagram for tranlsational maneuvers over an ellipsoid with a 5-h rotation period. Now we note that the symmetry between direct and retrograde maneuvers is lost and that the retrograde maneuvers have a wider region of stable transfer, as expected. Again, there is a significant destabilization when the body-fixed angular velocity is 1:1 synchronous with the natural frequency of hovering.

Conclusions

This paper discusses the stability of hovering and translational motion over a rotating small body, such as an asteroid or comet. The analysis assumes that the spacecraft is equipped with an altimeter and that a simple feedback control loop commands thrusting to keep the altimeter output constant. Hovering over a uniformly rotating body was investigated and found to be stable within a region closer than the resonance radius for the point mass body case, and within the equivalent distance for the case of an arbitrary body. The robustness of a hovering trajectory with respect to controller error increases as the hovering position becomes closer to the body.

Hovering over a nonuniformly rotating body was also investigated, with both general and specific cases studied. In this case, the stability of hovering is similar in many respects to hovering over a uniformly rotating body, but the regions of stability are diminished due to resonances between the body's precession and natural frequencies of motion.

Finally, the stability of translational motion over a small body while implementing the hovering control was investigated. In some special cases, this problem can be analyzed using the simpler theory of stationary hovering. For translational motion about a more general gravity field, the problem becomes similar to the computation of periodic orbit stability. In both cases, preferred directions of translation can be defined, generally in the opposite direction of the small-body rotation. Some numerical surveys of this problem were made that established connections between instabilities in these transfers and resonances between the angular rate of a maneuver and the natural frequency of a stabilized, hovering spacecraft.

Acknowledgments

The work described here was funded in part by the Telecommunications and Mission Operations Directorate Technology Program

by a grant from the Jet Propulsion Laboratory, California Institute of Technology, which is under contract with NASA. Support for S. Sawai was from a Fellowship from the Ministry of Education, Japan.

References

[1]Scheeres, D. J., Williams, B. G., and Miller, J. K., "Evaluation of the Dynamic Environment of an Asteroid: Applications to 433 Eros," *Journal of Guidance, Control, and Dynamics*, Vol. 23, No. 3, 2000, pp. 466–475.

[2]Scheeres, D. J., "Stability of Hovering Orbits Around Small Bodies," American Astronautical Society, AAS Paper 99-159, Feb. 1999.

[3]Kawaguchi, J., Fujiwara, A., and Sawai, S., "Sample and Return Mission from Asteroid Nereus via Solar Electric Propulsion," *Acta Astronautica*, Vol. 38, No. 2, 1996, pp. 87–101.

[4]Hudson, R. S., and Ostro, S. J., "Shape of Asteroid 4769 Castalia (1989 PB) from Inversion of Radar Images," *Science*, Vol. 263, No. 5149, 1994, pp. 940–943.

[5]Harris, A. W., "Tumbling Asteroids," *Icarus*, Vol. 107, No. 1, 1994, pp. 209–211.

[6]Cesari, L., *Asymptotic Behavior and Stability Problems in Ordinary Differential Equations*, 2nd ed., Springer-Verlag, New York, 1963, pp. 55–59.